Cardiovasc Intervent Radiol (2019) 42:1449–1458
https://doi.org/10.1007/s00270-019-02286-7

CLINICAL INVESTIGATION IMAGING

Application of a Metal Artifact Reduction Algorithm for C-Arm Cone-Beam CT: Impact on Image Quality and Diagnostic Confidence for Bronchial Artery Embolization

Arne Estler[1] · Malte Bongers[1] · Christoph Thomas[2] · Gerald Hefferman[1,3] · Johannes Hofmann[1] · Rüdiger Hoffmann[1] · Konstantin Nikolaou[1] · Ulrich Grosse[1] · Gerd Grözinger[1]

Received: 9 April 2019 / Revised: 18 June 2019 / Accepted: 5 July 2019 / Published online: 18 July 2019

Abstract

Objective The objective of this study was to evaluate the potential benefit of a dedicated cone-beam-CT streak metal artifact removal technique (SMART) in terms of both image quality and diagnostic confidence in patients undergoing bronchial artery embolization.

Methods A total of 17 patients were included in this retrospective study. The SMART algorithm was applied to images containing streak artifacts generated by a radiopaque intra-arterial catheter tip. Quantitative evaluation of artifact severity was performed via measurement of the Hounsfield units along a closed loop surrounding the catheter tip and was conducted in the frequency domain following the application of the discrete Fourier transform to the measured data. A high proportion of power in the low frequencies of the resulting spectrum indicated a high level of streak artifacts. Qualitative evaluation of diagnostic confidence was performed using a 4-point Likert scale.

Results Both quantitative and qualitative evaluation demonstrated a significant reduction in artifact severity using the SMART algorithm. Quantitative evaluation demonstrated a mean artifact reduction of 22.5% using SMART compared to non-SMART images ($p < 0.001$). Qualitative evaluation demonstrated the greatest artifact reduction at the inner and outer aortic curvature, as well as immediately surrounding the tip of the catheter. In 6 of 17 cases, the use of the SMART algorithm yielded additional clinical information, increasing mean diagnostic confidence from 3.17 to 3.78 ($p < 0.001$).

Conclusion The SMART algorithm allows for efficient reduction of metal artifacts introduced by radiopaque catheter tips during cone-beam CT. Using this algorithm, diagnostic images of the aortic arch were significantly improved both quantitatively and qualitatively, yielding clinically relevant levels of enhanced diagnostic confidence. These results demonstrate that the SMART algorithm improves diagnostic and clinical characterization of the course of bronchial arteries on CBCT images, potentially improving the accuracy and clinical efficacy of bronchial artery embolization.

Level of Evidence 3.

Introduction

The clinical relevance of pulmonary hemorrhage is beyond doubt; mortality rates ranging from 7 to 18% have been reported for patients with intermittent hemoptysis, rates that rise to 45% in patients with acute hemoptysis [1–3]. Hemoptysis is a potentially life-threatening condition that is often caused by severe underlying pulmonary disease. The vascular origin of pulmonary hemorrhage is most commonly the bronchial arteries, followed in descending

✉ Arne Estler
arne.estler@med.uni-tuebingen.de

[1] Department of Diagnostic and Interventional Radiology, University Hospital Tuebingen, Hoppe-Seyler-Strasse 3, 72076 Tübingen Germany

[2] Department of Diagnostic and Interventional Radiology, University Hospital Duesseldorf, Moorenstr. 5, 40225 Düsseldorf Germany

[3] The Warren Alpert Medical School of Brown University, 222 Richmond St., Providence RI 02903, USA

order of likelihood by the intercostal arteries, pericardial phrenic arteries, and collaterals from the internal mammary arteries [4]. For decades, open surgery was the main therapy in patients with hemorrhage from these locations. Presently, these surgical approaches have largely been supplanted by endovascular bronchial artery embolization (BAE), which has been demonstrated to be both less invasive and produce superior patient outcomes relative to surgical intervention [4–7].

C-arm-based cone-beam CT (CBCT) is an imaging technology that has found utility as a means of supplementing fluoroscopic angiography during endovascular procedures. CBCT has become a valuable imaging modality for hepatic interventions such as transarterial chemoembolization (TACE), selective internal radiation therapy (SIRT), and transjugular intrahepatic portosystemic shunt (TIPS) procedures [8–10], as well as extrahepatic interventions such as prostate artery embolization [11]. More recently, intraprocedural CBCT has been used during BAE procedures in order to facilitate the detection and characterization of target bronchial arteries, a diagnostic task that can be challenging using fluoroscopy alone [12].

CBCT images are generated using flat-panel (FP) detectors mounted on mobile C-arms, allowing for rotational projection data acquisition and multi-planar image reconstruction in arbitrary planes in a manner analogous to multi-detector computed tomography (MDCT) [13]. The resulting cross-sectional images provided by CBCT provide valuable data for peri-procedural planning and help facilitate the navigation of intravascular catheters to target sites. However, limiting factors confounding the identification of bronchial arteries on CBCT images exist, reducing the diagnostic utility of CBCT in this clinically important context. Chief among these is the presence of streak artifacts caused by the presence of either a radiodense catheter tip or highly concentrated iodinated contrast agent in an area of clinical interest. This limitation severely reduces the image quality, diagnostic confidence, and clinical utility provided by CBCT images [14].

Metal artifacts are typically caused by beam hardening and subsequent photon starvation, resulting in excessive quantum noise [15]. The filtered back-projection reconstruction algorithm, by intensifying these nonlinear effects, leads to alternating dark and bright streak artifacts radiating from the radiodense catheter tip [15–17]. Structures adjacent to the source of the streak artifact can be masked or even completely obscured; the closer relevant anatomical structures are to the artifact source, the more the clinical utility of the resulting images is impaired.

The streak metal artifact reduction technique (SMART) algorithm was designed to reduce the deleterious impact of streak artifacts on image quality, potentially improving the diagnostic yield of CBCT during BAE [18]. Since bronchial arteries are often small and difficult to detect even in cases of optimal cross-sectional image quality, changes in tissue attenuation must be clearly visible in order to assess the origin and branching of these vessels. The aim of this study was to assess whether the SMART algorithm is an effective means of surmounting the technical and clinical limitations introduced by streak artifacts in the context of CBCT during BAE. In order to achieve this aim, quantitative evaluation of changes in artifact severity and qualitative evaluation of changes in diagnostic confidence resulting from the use of the SMART algorithm were performed.

Materials and Methods

Patient Selection

This was an institutional ethics board-approved retrospective study. Inclusion criteria for transarterial BAE were as follows:

1. Patients with hemorrhage from a bronchial artery caused by a range of pathologies, including recurrent bronchial bleeding with or without an underlying tumor, arteriovenous malformation, or bleeding due to an unknown cause;
2. Patients aged 18 years or older;
3. And patients with pre-procedural CT examinations, selective aortic and bronchial angiograms, and corresponding CBCT images available for retrospective review.

Enrolled patients were treated between 11/2016 and 03/2018 (mean age: 64.6 ± 14.6, age range 26–86, 59% male). Ultimately, 17 patients who underwent BAE during this time period were included. Each patient gave informed consent for study inclusion. All patients underwent CBCT imaging during the angiographic work-up of BAE in order to visualize the bronchial arteries, followed by subsequent selective angiography and BAE.

Image Acquisition

All imaging was performed using a single angiographic system (Artis Zeego, Siemens Healthcare GmbH, Forchheim, Germany). After transfemoral access was gained using a 4F sheath, a 4F pigtail catheter with a radiopaque tip (Cordis, Tipperary, Ireland) was placed in the aortic arch for angiography and CBCT. CBCT images were acquired after the administration of diluted contrast medium (50% dilution with saline with a maximum of 40 mL Ultravist 370 per patient at a flow rate of 10 mL/s for 8 s)

followed by a saline flush injected by an automated power injector (Accutron-HP-D, Medtron, Saarbrücken, Germany). Contrast administration was begun 2 s before the start of the C-arm rotation. The rotation time for CBCT was 6 s, and images were acquired at a rate of 60 frames/s. The system acquired 397 projection images with a detector entrance dose of 0.36 μGy/frame and an angular increment of 0.5°/frame on a 200° circular trajectory around the patient. CBCT was acquired using breath-holding technique. The source power was 90 kVp, and the field of view was 48 cm with a voxel matrix of 512 × 512.

All acquired projection data were transferred from the Artis Workplace to a dedicated research workstation (Syngo X Workplace [XWP], X VB21B P05 Rev.7; Siemens Healthcare GmbH, Forchheim, Germany) for post-processing using the SMART algorithm. The SMART algorithm was applied in using the same process as described in the previous literature [19]. The uncorrected volume with artifacts was reconstructed, and CT-like axial images with an isotropic voxel size of 0.5 mm were reconstructed using a filtered back-projection algorithm. Next, the SMART algorithm was applied to the reconstructed volume. This step required manual segmentation of the volume containing streak artifacts from the artifact-free volume in the uncorrected data set. The projection data were then reconstructed a second time in which the segmented volumes of interest (VOI) and uncorrected volumes without streak artifact were combined with an isotropic voxel size of 0.5 mm using filtered back-projection (FBP) using a soft tissue kernel.

Quantitative Evaluation of Image Quality

In order to quantify artifact severity, a dedicated in-house software program was utilized and implemented in MATLAB (MathWorks, Natick, MA, USA) as described in the previous literature [20, 21]. Three regions of interest (ROIs) consisting of contiguous loops of polygonal lines were marked on axial slices, the first surrounding the tip of the radiopaque catheter within the aortic arch (ROI 1), the second surrounding the proximal descending aorta (ROI 2), and the third surrounding the distal descending aorta (ROI 3), as pictured in Figs. 1 and 2. The same procedure was performed for both corrected (with SMART) and uncorrected (without SMART) data sets. ROIs 2 and 3 both served as control groups, as the SMART algorithm was applied only to the data which included ROI 1 at the level of the aortic arch. The Hounsfield unit (HU) values of the voxels crossed by the polygonal lines of the ROIs were gathered and considered as a vector in the distance domain. The discrete Fourier transformation was applied to the resulting vector in order to quantify the relative power of the frequencies of density change along the defined polygonal lines. CBCT metal artifacts, with their characteristic streak appearance, result in increased power in the low-frequency range of the resulting spectrum; normal image noise contributes power at higher frequencies. Thus, the Fourier coefficients representing the power at lower frequencies were analyzed and compared between the SMART-corrected and non-SMART-corrected images.

Qualitative Evaluation of Diagnostic Confidence

In order to qualitatively assess changes in both image quality and diagnostic confidence resulting from the use of the SMART algorithm, images were reviewed by two board-certified interventional radiologists, both of whom had at least five years of professional experience in BAE and chest CT imaging, using a consensus reading approach. Neither reader was involved in the initial treatment of the patients, and the two readers were blinded both to the clinical cases and to the presence or absence of the application of the SMART algorithm for each image. In order to further reduce the bias in the assessment of diagnostic confidence, the studies were shown to the readers in a random order without access to corresponding subsequent imagery. A Likert scale was used for subjective scoring of image quality: a score of 0 corresponded to no artifacts, 1 to slight artifacts, 2 to moderate artifacts, and 3 to strong artifacts as previously described for streak artifact evaluation [22]. A second Likert scale was used for the subjective assessment of diagnostic confidence in the same manner as was reported in prior literature by Grosse et al. [12] in which 1 corresponded to very low confidence, 2 to low confidence, 3 to moderate confidence, 4 to high confidence, and 5 to very high confidence. Five different anatomic regions (left subclavian artery, brachiocephalic trunk, greater curvature of the aorta, lesser curvature of the aorta, and descending aorta) were specifically evaluated. After blinded artifact evaluation, clinically relevant additional findings were additionally recorded.

Statistical Analysis

For statistical analysis of the quantitative artifact severity data, Student's t test was applied using JMP software (JMP version 8.01, SAS Institute, Cary, NC, USA). Results demonstrating a p value of less than 0.05 were considered significant. Results are displayed as mean ± standard deviation. Median values and interquartile ranges were calculated for subjective artifact evaluation and level of diagnostic confidence. The Kruskal–Wallis test was used for evaluation of subjective artifact evaluation.

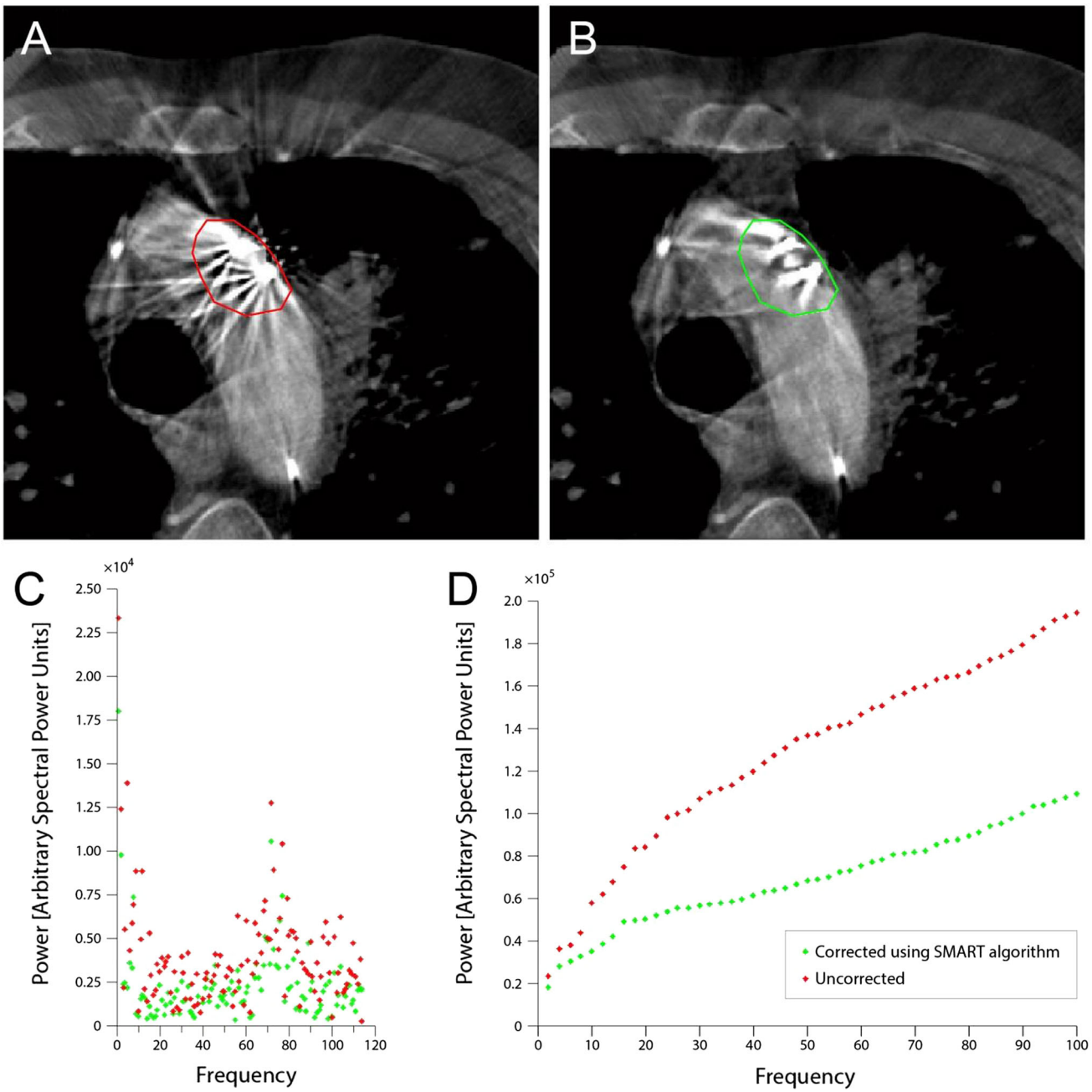

Fig. 1 Representative image demonstrating ROI 1 at the level of the radiopaque catheter tip: **A** uncorrected CBCT image with polygonal ROI 1 vector marked in red; **B** the same CBCT image after application of the SMART algorithm with ROI 1 vector marked in green; **C** results of the application of the discrete Fourier transform on both uncorrected (red) and SMART-corrected (green) ROI 1 vector data; and **D** the cumulative power as a function of frequency for both uncorrected (red) and SMART-corrected (green) frequency-domain data. Higher power in the low-frequency components of the uncorrected data vs. the SMART-corrected data demonstrates quantitative reduction of streak artifact intensity after application of the SMART algorithm

Results

Quantitative Analysis of Image Quality

In total, 24 bronchial arteries were evaluated in 17 patients. Quantitative image analysis results are shown in Figs. 1, 2 and 3. These results demonstrated the highest artifact density in the region of the tip of the angiographic catheter and significantly lower artifact density in the other two regions (ROI $1_{\text{non-SMART}}$: $2.107 \times 10^6 \pm 5.09 \times 10^4$ vs. ROI $2_{\text{non-SMART}}$: $1.347 \times 10^6 \pm 3.95 \times 10^4$ vs. ROI $3_{\text{non-SMART}}$: $1.136 \times 10^6 \pm 3.6 \times 10^4$). The artifacts originating from the catheter tip were significantly reduced in the images processed using the SMART algorithm; artifact

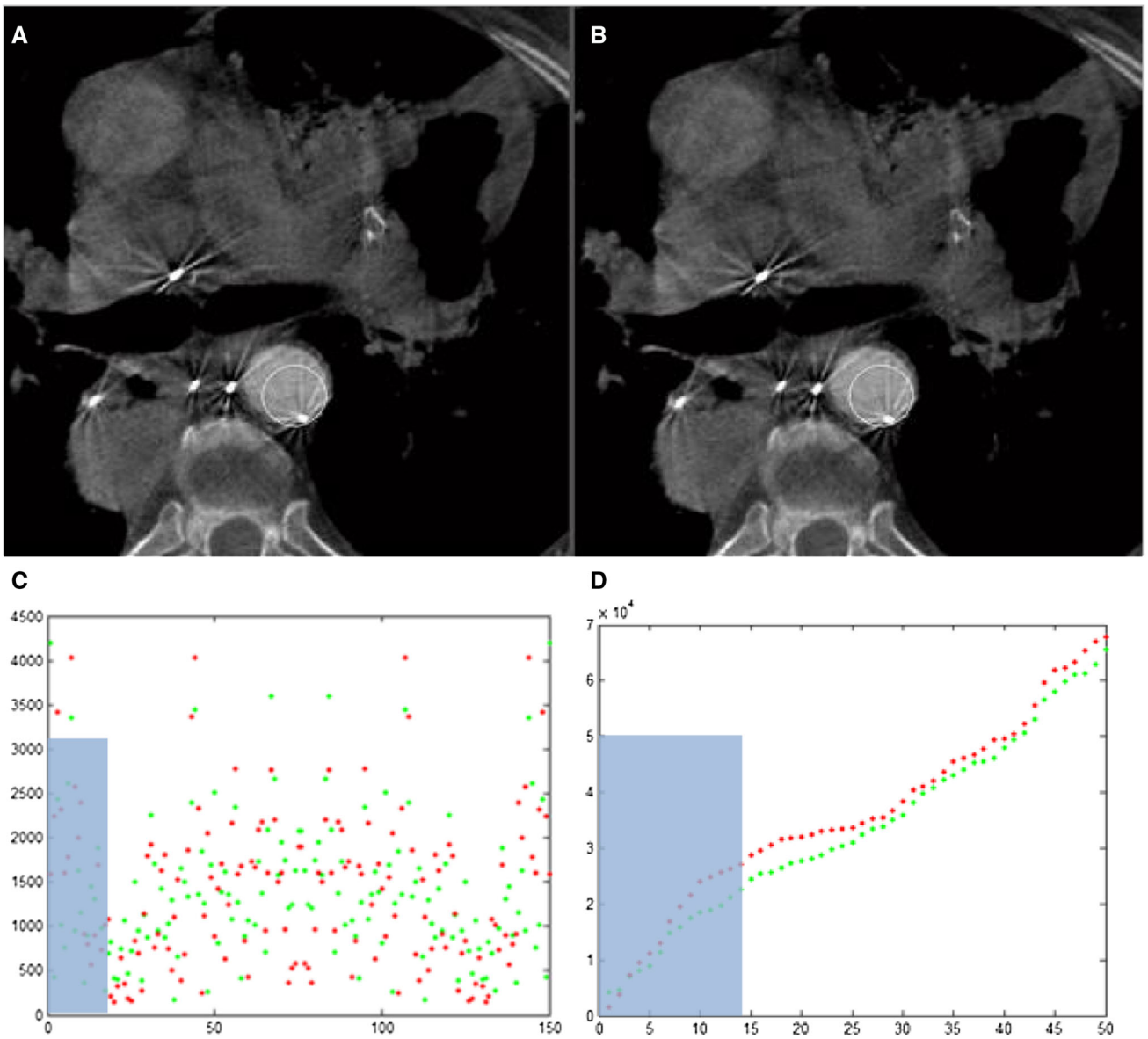

Fig. 2 Representative image demonstrating ROI 3 at the level of distal descending aorta: **A** uncorrected CBCT image with polygonal ROI 3 vector marked in red; **B** the same CBCT image after application of the SMART algorithm with ROI 3 vector marked in green; **C** results of the application of the discrete Fourier transform on both uncorrected (red) and SMART-corrected (green) ROI 3 vector data; and **D** the cumulative power as a function of frequency for both uncorrected (red) and SMART-corrected (green) frequency-domain data. In contrast to Fig. 1, no radiopaque catheter tip is present at this level, which served as a control region; consequently, no significant difference was observed in the low-frequency components of the data before and after application of the SMART algorithm

amplitudes were suppressed by an average of 22.5% (ROI 1_{SMART}: 1.63×10^6 vs. ROI $1_{non\text{-}SMART}$: 2.107×10^6, $p < 0.001$), while the artifacts did not differ significantly at the other locations (ROI 2_{SMART}: 1.27×10^6 vs. ROI $2_{non\text{-}SMART}$: 1.347×10^6, $p = 0.494$; ROI 3_{SMART}: 1.06×10^6 vs. ROI $3_{non\text{-}SMART}$: 1.136×10^6, $p = 0.415$).

Qualitative Analysis of Beam Hardening Artifacts

The results of the qualitative image analysis and subjective level of diagnostic confidence are shown in Table 1. These results demonstrated differing degrees of subjective artifact reduction due to the application of the SMART algorithm in different anatomical regions. Significant reductions were observed at the greater curvature of the aortic arch ($mean_{SMART}$:1.3 vs. $mean_{non\text{-}SMART}$: 2.1, $p = 0.005$; $median_{SMART}$: 1 vs. $median_{non\text{-}SMART}$: 2), the lesser

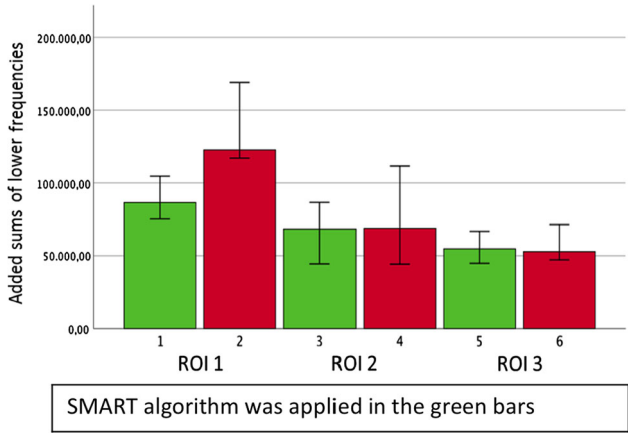

Fig. 3 Comparison of the cumulative power in the low-frequency components of the data from ROIs 1, 2, and 3 before application of the SMART algorithm (red) and after application (green). High levels of cumulative power in the low frequencies correspond to high levels of streak artifact severity. A significant decrease was observed in ROI 1 at the level of the radiopaque catheter tip; no changes were observed at the level of the control regions (ROIs 2 and 3)

curvature of the aortic arch ($mean_{SMART}$: 1.2 vs. $mean_{non\text{-}SMART}$: 2.1, $p < 0.001$, $median_{SMART}$: 1 vs. $median_{non\text{-}SMART}$: 2), and at the level of the radiodense catheter tip ($mean_{SMART}$: 2.5 vs. $mean_{non\text{-}SMART}$: 3.8, $p < 0.001$; median from 3 to 4). Examples of this artifact reduction are shown in Fig. 4. No significant changes were observed at the level of the subclavian artery ($p = 0.082$), the brachiocephalic trunk ($p = 0.157$), and the descending aorta ($p = 0.317$).

Additional Findings

Mean and standard deviation of the dose area product of the CBCTs were 2281 μGm^2 and 1315 μGm^2, respectively. In 35% (6/17 cases) of cases, application of the SMART algorithm resulted in the detection of additional clinically relevant findings. Examples of these additional findings include: determining the exact course of the bronchial artery from origin to periphery; observation of the course of the intercostobronchial trunk, which was not visible in the non-SMART images; and increased visibility of feeder vessels. Representative images demonstrating these clinically relevant findings are shown in Fig. 5.

Discussion

There exists a broad spectrum of anatomic variation of the branches and feeding vessels of the bronchial arteries. Consequently, both a high level of diagnostic experience and advanced imaging techniques are required to support the interventionalist during BAE procedures. This study demonstrates that the SMART algorithm facilitates the detection of the bronchial arteries by reducing the streak artifacts induced by a radiopaque catheter tip (Fig. 6).

CBCT is fast becoming a critical peri-interventional diagnostic tool during complex endovascular procedures. A recent study by Grosse et al. [12] showed that CBCT imaging similarly facilitates BAE procedures, allowing for more rapid intraprocedural detection of target arteries. This enhanced detection decreased the duration of the intervention, positively impacting procedural efficiency and patient safety. However, the peri-procedural nature of CBCT necessitates the presence of radiopaque catheter tips and contrast media in the aorta during image acquisition, resulting in the generation of streak artifact in the area of greatest diagnostic importance. These artifacts reduce diagnostic accuracy, particularly when characterizing the wall of the aorta at the inner curvature of the aortic arch, the precise area from which the bronchial arteries most commonly arise.

High-quality imaging of the wall of the aorta and its branches is crucial for this technically demanding procedure, since these branching arteries demonstrate a broad range of physiologic variations. The loss of critical anatomical information due to reduced image quality may

Table 1 Results of qualitative evaluation of images with and without application of the SMART algorithm

Anatomical region (Likert-scale range)	Mean value without SMART	Mean value with SMART	*p* value
Subclavian artery (image quality 0–3)	0.9	0.7	0.082
Brachiocephalic trunk (image quality 0–3)	1.4	1.1	0.157
Greater curvature (image quality 0–3)	2.1	1.3	0.005
Lesser curvature (image quality 0–3)	2.1	1.2	< 0.001
Descending aorta (image quality 0–3)	0.9	0.8	0.317
Tip of radiopaque catheter (diagnostic confidence 1–5)	3.8	2.5	< 0.001

A Likert scale range of 0–3 was used to assess image quality for all anatomical regions with the exception of the region which included the radiopaque catheter tip. In this region, diagnostic confidence to rule out bronchial arteries was assessed with a 1–5 Likert scale, in the same manner as reported in prior work by Grosse et al.

p values < 0.05 were considered significant

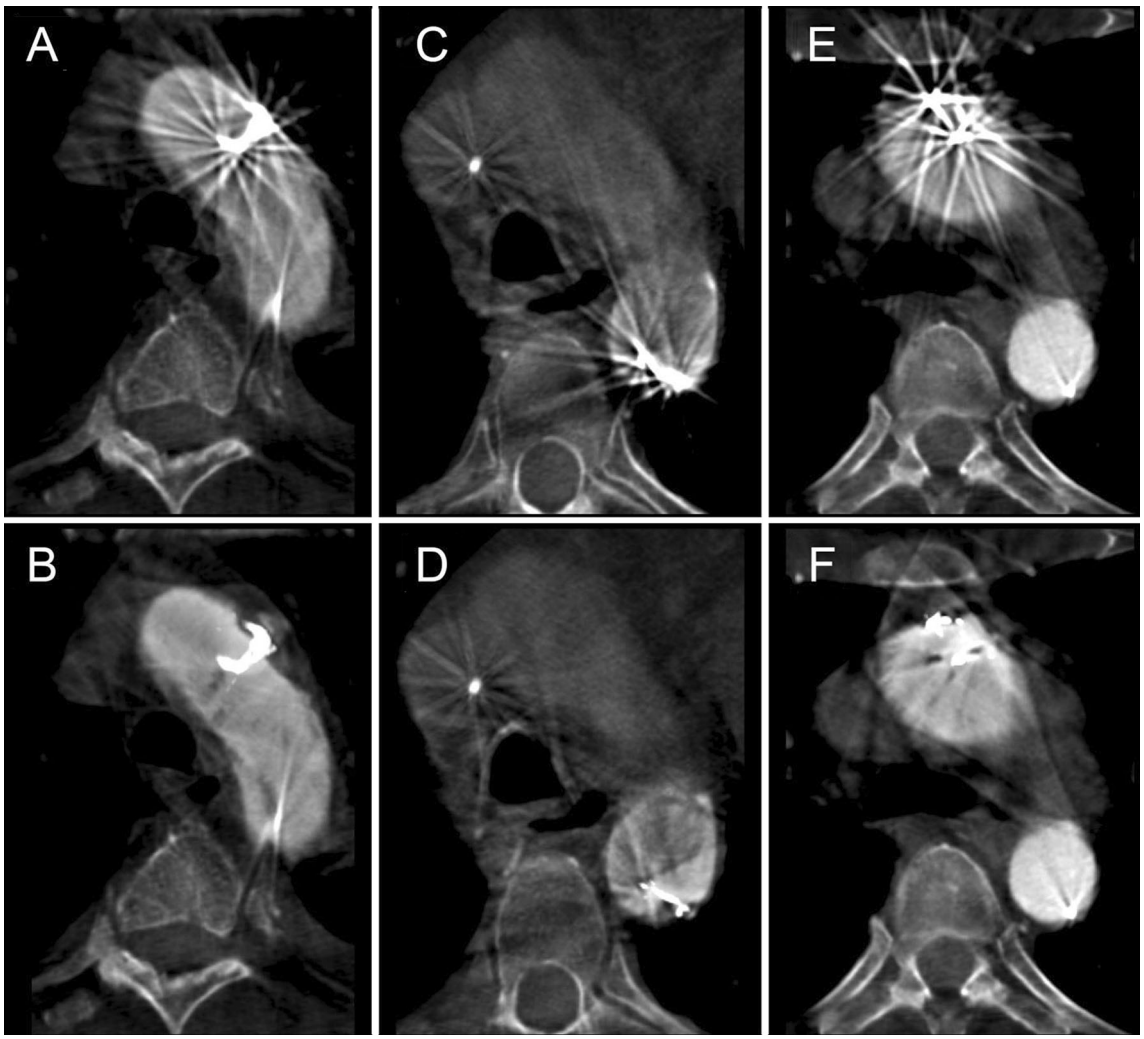

Fig. 4 Representative images from three patients at the level of the aortic arch that include streak artifact due to the presence of a radiopaque catheter tip: **A**, **C**, **E** uncorrected CBCT images; and **B**, **D**, **F** the same images after application of the SMART algorithm

prolong procedure time, result in the embolization of non-target branches, or make a treatment impossible, resulting in diminished procedural efficacy, reduced patient safety, and increased cost. This is particularly true in demanding cases involving patients with rare anatomic variations of the bronchial vessels and cases in which the exact determination of target vessels, and the exclusion of aberrant bronchial arteries is essential.

MDCT imaging is a closely related imaging modality that is susceptible to similar artifacts inducted by radiopaque objects. Corrective algorithms, such as iterative metal artifact reduction (IMAR) and dual-energy metal artifact reduction (DEMAR), are already broadly used in MDCT imaging in order to minimize the deleterious effects of streak artifacts on diagnostic confidence [20]. Similar techniques have been successfully employed in the field of interventional neuroradiology in which metal artifact reducing (MAR) algorithms have been shown to increase the visibility of hemorrhage, brain parenchyma, and vessels after metallic stent and coil placement [14, 23, 24]. These algorithms are based on a similar method as the SMART algorithm employed in this study, which uses a nonlinear interpolation procedure to reduce streak artifacts [14]. Metal artifacts in raw CBCT data are automatically detected by these segmentation algorithms, further simplifying algorithmic handling [23].

Several scientific approaches have been used to quantify the severity of metallic streak artifacts in the related case of MDCT. A number of studies defined ROIs in two areas (near field and far field) where the most pronounced streak artifacts were observed [22, 25, 26]. The artifacts were not quantified objectively, but rather relied on observer-defined measurements based on Hounsfield units at several distances from the artifact source. This approach is vulnerable to vagaries introduced by the subjective perception of a specific artifact; consequently, results of this measurement

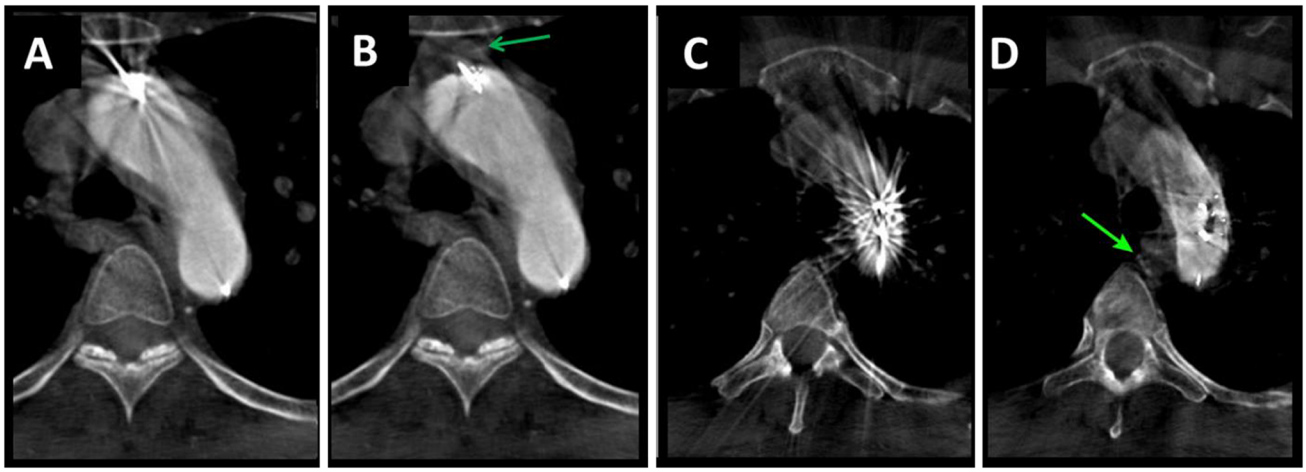

Fig. 5 Representative images from two patents showing clinically relevant improvement in the identification of variant courses of the bronchial arteries after application of the SMART algorithm: **A** uncorrected image from a patient with an aberrant bronchial artery arising from the brachiocephalic trunk with a course ventral to the aortic arch; **B** the same image after application of the SMART algorithm with the variant anatomy marked with a dark green arrow; **C** uncorrected image from a patient with an aberrant bronchial artery running medial the aortic arch; and **D** the same images after application of the SMART algorithm with variant anatomy marked with a green arrow. In 9 of 17 cases, the subjective amount of artifacts was substantially reduced and the arterial wall at the level of the expected origin of the bronchial arteries was more clearly visible, allowing for the exclusion of aberrant vessel origins with high confidence

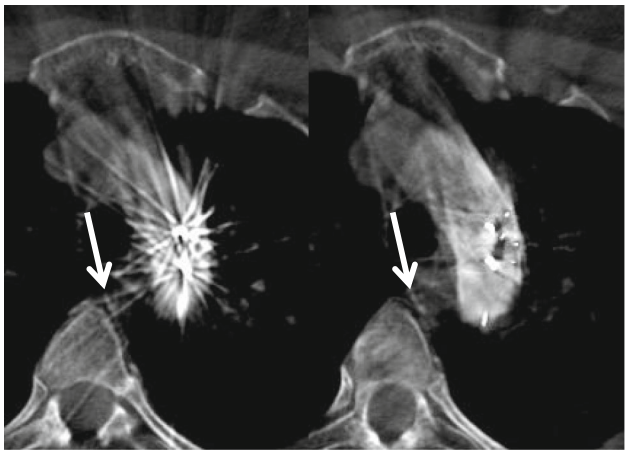

Fig. 6 Example of patients with clinically relevant findings demasked with the SMART algorithm and therefore result in a clinical relevant improvement. Patient with aberrant bronchial artery running medial the aortic arch (with arrow in **A** and **B**): **A** without SMART and **B** with SMART

approach cannot be consistently repeated using a multi-reader approach. In contrast, this study utilizes an artifact quantification method that has been demonstrated in prior published literature to be an effective, reproducible method of artifact measurement [20, 21]. This method measures the apparent Hounsfield unit density of a continuous loop of voxels surrounding an artifact source. The use of a discrete Fourier transform on the resulting data vector allows for a reliable and non-operator-dependent quantification of artifact severity [20, 21]. The reliability of this approach was observed to be similar to that demonstrated in prior work and is perhaps best demonstrated by the fact that the artifact-free ROIs 2 and 3 demonstrated no significant difference between SMART and non-SMART images.

Interventionalists have alternative tools at their disposal in order to reduce streak artifacts during CBCT imaging. The simplest of these strategies is the use of an angiographic catheter without a radiopaque tip. However, this approach comes at the cost of reduced visibility of catheter position during fluoroscopic imaging and may require the interventionalist to directly remove the catheter tip during angiographic intervention as the majority of intravascular catheters come equipped with radiopaque tips by default. Furthermore, other sources of streak artifact exist, including concentrated contrast media within the distal catheter or exiting the catheter tip, sternotomy wires, and pacemaker leads, to name a few.

This study has several limitations. Firstly, the retrospective design of the study may limit the ability of the resulting data to be directly extrapolated to expected improvements in clinical outcomes for patients undergoing CBCT for BAE. Secondly, the number of patients is relatively limited, and in none of the cases was a bronchial artery completely missed during intervention because of the presence of metallic streak artifacts. A practical limitation of the algorithm as currently implemented is that the SMART algorithm is applied only after initial reconstruction of the CBCT raw data is complete. This step usually takes several minutes depending on the experience level of the interventionalist and also depends heavily on computer capacity [27]. However, as cannulation of the desired artery during BAE usually is the most time-consuming

element of the procedure, the additional time needed to apply the SMART algorithm to CBCT data may be compensated by faster vessel cannulation and enhanced diagnostic confidence. Nevertheless, automatic implementation of the algorithm during image acquisition and reconstruction would likely shorten the procedure time, further enhancing the clinical utility of the SMART algorithm.

To conclude, application of the SMART algorithm allows for quantitatively and qualitatively improved CBCT image quality in the presence of streak artifact, facilitating the assessment of critical vascular structures during BAE and potentially benefiting both interventionalists and the patients in their care.

Compliance with Ethical Standards

Conflict of interest The authors declare that they have no conflict of interest.

References

1. Knott-Craig CJ, Oostuizen JG, Rossouw G, Joubert JR, Barnard PM. Management and prognosis of massive hemoptysis: recent experience with 120 patients. J Thorac Cardiovasc Surg. 1993;105:394–7.
2. Gourin A, Garzon AA. Operative treatment of massive hemoptysis. Ann Thorac Surg. 1974;18:52–60.
3. Ittrich H, Klose H, Adam G. Radiologic management of haemoptysis: diagnostic and interventional bronchial arterial embolisation. RoFo 2015;248–59.
4. Palade E. Management of hemoptysis: results of an algorithm-based interdisciplinary treatment scheme. Zentralbl Chir. 2016;141:85–92.
5. Remy J, et al. Treatment, by embolization, of severe or repeated hemoptysis associated with systemic hypervascularization. Nouv Press Med. 1973;2:2060.
6. Tom LM, Palevsky HI, Holsclaw DS, Trerotola SO, Dagli M, Mondschein JI, et al. Recurrent bleeding, survival, and longitudinal pulmonary function following bronchial artery embolization for hemoptysis in a U.S. adult population. J Vasc Interv Radiol. 2015;26:1806–13.
7. Garcia-Olivé I, Sanz-Santos J, Centeno C, Andreo F, Muñoz-Ferrer A, Serra P, et al. Results of bronchial artery embolization for the treatment of hemoptysis caused by neoplasm. J Vasc Interv Radiol. 2014;25:221–8.
8. Ketelsen D, Groezinger G, Maurer M, Lauer UM, Grosse U, Horger M, et al. Three-dimensional C-arm CT-guided transjugular intrahepatic portosystemic shunt placement: feasibility, technical success and procedural time. Eur Radiol. 2016;26:4277–83.
9. Grözinger G, Kupferschläger J, Dittmann H, Maurer M, Grosse U, La Fougère C, et al. Assessment of the parenchymal blood volume by C-arm computed tomography for radioembolization dosimetry. Eur J Radiol. 2016;85:1525–31.
10. Syha R, Grozinger G, Grosse U, Maurer M, Zender L, Horger M, et al. Parenchymal blood volume assessed by c-arm-based computed tomography in immediate posttreatment evaluation of drug-eluting bead transarterial chemoembolization in hepatocellular carcinoma. Invest Radiol. 2016;51:121–6.
11. Teichgräber U, Aschenbach R, Diamantis I, von Rundstedt FC, Grimm MO, Franiel T. Prostate artery embolization: indication, technique and clinical results. RoFo. 2018;190(9):847–55. https://doi.org/10.1055/a-0612-8067.
12. Grosse U, Grözinger G, Syha R, Ketelsen D, Partovi S, Nikolaou K, et al. Intra-procedural bronchial artery embolization planning: the usefulness of cone-beam CT. Acta Radiol. 2019. https://doi.org/10.1177/0284185119837931.
13. Kalender WA. The use of flat-panel detectors for CT imaging. Radiologe. 2003;43:379–87.
14. Psychogios MN, Scholz B, Rohkohl C, Kyriakou Y, Mohr A, Schramm P, et al. Impact of a new metal artefact reduction algorithm in the noninvasive follow-up of intracranial clips, coils, and stents with flat-panel angiographic CTA: initial results. Neuroradiology. 2013;55:813–8.
15. Prell D, Kyriakou Y, Struffert T, Dörfler A, Kalender WA. Metal artifact reduction for clipping and coiling in interventional C-Arm CT. Am J Neuroradiol. 2010;31:634–9.
16. Prell D, Kalender WA, Kyriakou Y. Development, implementation and evaluation of a dedicated metal artefact reduction method for interventional flat-detector CT. Br J Radiol. 2010;83:1052–62.
17. Prell D, Kyriakou Y, Kachelrie M, Kalender WA. Reducing metal artifacts in computed tomography caused by hip endoprostheses using a physics-based approach. Invest Radiol. 2010;45:747–54.
18. Shellikeri S, Girard E, Setser R, Bao J, Cahill AM. Metal artefact reduction algorithm for correction of bone biopsy needle artefact in paediatric C-arm CT images: a qualitative and quantitative assessment. Clin Radiol. 2016;71:925–31.
19. Meyer M, Kalender WA, Kyriakou Y. A fast and pragmatic approach for scatter correction in flat-detector CT using elliptic modeling and iterative optimization. Phys Med Biol. 2010;55:99–120.
20. Bongers MN, Schabel C, Thomas C, Raupach R, Notohamiprodjo M, Nikolaou K, et al. Comparison and combination of dual-energy- and iterative-based metal artefact reduction on hip prosthesis and dental implants. PLoS One. 2015;10(11):e0143584. https://doi.org/10.1371/journal.pone.0143584.
21. Mangold S, Gatidis S, Luz O, König B, Schabel C, Bongers MN, et al. Single-source dual-energy computed tomography: use of monoenergetic extrapolation for a reduction of metal artifacts. Invest Radiol. 2014;49(12):788–93. https://doi.org/10.1097/RLI.0000000000000083.
22. Hamie QM, Kobe AR, Mietzsch L, Manhart M, Puippe GD, Pfammatter T, et al. Prototype metal artefact reduction algorithm in flat panel computed tomography—evaluation in patients undergoing transarterial hepatic radioembolisation. Eur Radiol. 2018;28:265–73.
23. Pjontek R, Önenköprülü B, Scholz B, Kyriakou Y, Schubert GA, Nikoubashman O, et al. Metal artifact reduction for flat panel detector intravenous CT angiography in patients with intracranial metallic implants after endovascular and surgical treatment. J Neurointerv Surg. 2016;8(8):824–9. https://doi.org/10.1136/neurintsurg-2015-011787.
24. Mennecke A, Svergun S, Scholz B, Royalty K, Dörfler A, Struffert T. Evaluation of a metal artifact reduction algorithm applied to post-interventional flat detector CT in comparison to pre-treatment CT in patients with acute subarachnoid haemorrhage. Eur Radiol. 2017;27(1):88–96.
25. Finkenstaedt T, Morsbach F, Calcagni M, Vich M, Pfirrmann CWA, Alkadhi H, et al. Metallic artifacts from internal scaphoid fracture fixation screws: comparison between C-arm flat-panel, cone-beam, and multidetector computed tomography. Invest Radiol. 2014;49(8):532–9. https://doi.org/10.1097/RLI.0000000000000052.
26. Filli L, Marcon M, Scholz B, Calcagni M, Finkenstädt T, Andreisek G, et al. Evaluation of a prototype correction algorithm

to reduce metal artefacts in flat detector computed tomography of scaphoid fixation screws. Skeletal Radiol. 2014;43(12):1705–12. https://doi.org/10.1007/s00256-014-1986-3.

27. Stidd DA, Theessen H, Deng Y, Li Y, Scholz B, Rohkohl C, et al. Evaluation of a metal artifacts reduction algorithm applied to postinterventional flat panel detector CT imaging. Am J Neuroradiol. 2014;35:2164–9.